HTML ABSTRACT + LINKS

Space charge saturated sheath regime and electron temperature saturation in Hall thrusters

Y. Raitses,[a] D. Staack, A. Smirnov, and N. J. Fisch
Plasma Physics Laboratory, Princeton University, P. O. Box 451, New Jersey 08543

(Received 2 September 2005; accepted 5 September 2005; published online 7 July 2005)

Existing electron-wall interaction models predict that secondary electron emission in Hall thrusters is significant and that the near-wall sheaths are space charge saturated. The experimental electron-wall collision frequency is computed using plasma parameters measured in a laboratory Hall thruster. In spite of qualitative similarities between the measured and predicted dependencies of the maximum electron temperature on the discharge voltage, the deduced electron-wall collision frequency for high discharge voltages is much lower than the theoretical value obtained for space charge saturated sheath regime, but larger than the wall recombination frequency. The observed electron temperature saturation appears to be directly associated with a decrease of the Joule heating rather than with the enhancement of the electron energy loss at the walls due to a strong secondary electron emission. Another interesting experimental result is related to the near-field plasma plume, where electron energy balance appears to be independent on the magnetic field. © *2005 American Institute of Physics*. [DOI: 10.1063/1.1944328]

I. INTRODUCTION

The plasma-wall interaction in the presence of strong secondary electron or thermionic emission has been studied theoretically[1,2] and experimentally[3–5] both as a basic phenomenon and in relation to numerous plasma applications such as, for example, fusion devices.[4–7] The electron emission from the wall greatly reduces the sheath potential drop[1–4] and, thereby, weakens thermal insulating properties of the sheath.[1,5] When the flux of secondary electrons from the wall is approximately equal to the flux of primary electrons from the plasma, the sheath becomes space charge saturated (SCS). Any further increase of the secondary electron flux into the plasma is restricted by a potential minimum formed near the wall surface.[1,3]

A general description of the secondary electron emission (SEE) effects[1,2] on the plasma flow has been recently included in fluid models of Hall thrusters.[8–11] A Hall thruster is a plasma discharge device with crossed fields, which is used for spacecraft propulsion. In a Hall thruster, the axial electric and radial magnetic fields are applied in an annular ceramic channel. The electric field supplies energy mainly to accelerate the unmagnetized ions, but some energy goes also to heat the electrons, which diffuse across the radial magnetic field.[12,13] A typical Hall thruster operates in a sub-kilovolt discharge voltage range using xenon gas as a propellant. Recently Barral *et al.*[9] and Ahedo *et al.*,[10,11] within the framework of quasi-one-dimensional fluid Hall thruster models, predicted the dependence of the maximum electron temperature on the discharge voltage. The Joule heating increases with the applied discharge voltage and so does the electron energy loss at the walls, which becomes the dominant electron energy loss mechanism as the near-wall sheaths approach the space charge saturation.[9–11] In particular, the models by Barral *et al.* and Ahedo *et al.* suggest the occurrence of the SCS regime of Hall thruster operation at sufficiently high discharge voltages and show how the maximum electron temperature grows upon the transition from the non-SCS regime to the regime with the SCS near-wall sheaths. It is important to note also that strong SEE from the channel walls may affect oscillatory behavior of the thruster discharge and induce the near-wall conductivity.[9,13,14]

Our recent experiments showed that the local electron temperature increases fairly linearly with the local plasma potential inside the thruster channel and in the near-field plasma plume.[15] The electron temperature inside a boron nitride channel was almost two times larger than the critical value predicted for the SCS sheath regime under the assumption of Maxwellian electron energy distribution function (EDF).[15–18] Recent kinetic studies suggested that the effective SEE coefficient is reduced because wall losses depopulate the high energy tail of the electron EDF in a weakly collisional plasma of Hall thrusters.[17,19] A reduced SEE due to a depletion of electron EDF may occur similarly in the collisionless regime of a divertor operation in fusion devices.[20] However, the departure of the electron EDF from the Maxwellian does not necessarily mean that the SCS sheath regime is impossible in Hall thrusters. In fact, measurements of the thruster discharge characteristics[14] indirectly support the predicted transition to the SCS regime.[9] The transition to the SCS regime appears at the discharge voltages higher than those used in Ref. 15 (less than 400 V). We recently reported how the channel geometry (channel width) might affect the acceleration region in a Hall thruster.[16] An increase of the discharge voltage from 400 to 500 V caused almost no changes of the maximum electron temperature. This is in keeping with fluid models,[9–11] which predict saturation of the electron temperature due to SEE-enhanced wall energy losses. The location of the acceleration region was shown to be sensitive to the

[a]Electronic mail: yraitses@pppl.gov

 © 2005 American Institute of Physics

Downloaded 18 Jul 2005 to 198.35.4.202. Redistribution subject to AIP license or copyright, see http://pop.aip.org/pop/copyright.jsp

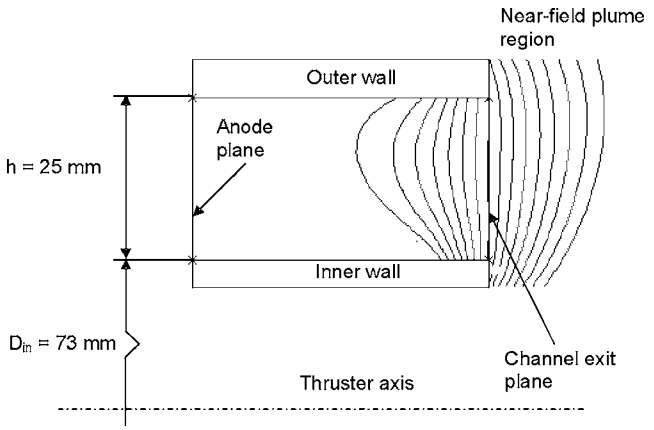

FIG. 1. Schematic of the thruster channel with superimposed magnetic field lines. The magnetic field distribution was simulated for the experimental conditions.

channel width, but not so much to the discharge voltage.

The present paper reports how Joule heating and electron cooling due to electron-wall interaction controls the electron temperature. In particular, the physical mechanisms causing the electron temperature saturation are investigated.

This paper is organized as follows. Section II describes experimental setup and procedure. Experimental results are presented in Sec. III, and their implications are discussed in Sec. IV. In Sec. V we summarize our main conclusions.

II. EXPERIMENT

A. Setup

The test facility and the thruster used in these experiments are described elsewere.[15,16,21,22] A 2 kW Hall thruster was operated at xenon gas flow of 19 sccm and constant electromagnet coil currents. The magnetic field distribution is shown in Fig. 1. During the thruster operation the background pressure in a 28 m^3 vacuum vessel equipped with cryopumps did not exceed 6 microtorr. The thruster channel was made of a grade HP boron nitride ceramic material. The diameters of the inner and outer channel walls are 73 and 123 mm, respectively. The channel length measured from the anode to the channel exit is 46 mm. A commercial hollow-cathode is used as a cathode-neutralizer to sustain the discharge and neutralize the charge and current of the ion beam. The cathode was placed a few centimeters away from the thruster symmetry axis to avoid the cathode bombardment by the energetic ions from the thruster.

The plasma potential and the electron temperature were deduced from the measurements of the floating potentials of the emissive and cold (non-emissive) Langmuir probes. Figure 2 shows a schematic of the probe setup. A positioning stage moves the probe rapidly back and forth along the channel median across the radial magnetic field.[15,16,21] The probe wire diameter is 0.1 mm. The probe has a segmented shield, which is made from equally spaced carbon ringlets that surround an alumina ceramic tube. The shield reduces plasma perturbations, which can be induced by high SEE from alumina ceramic.[21] For the results presented in this paper, the probe-induced changes of the discharge current were less than 15%.

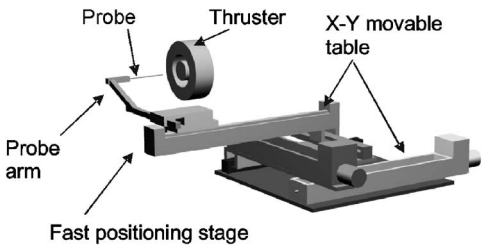

FIG. 2. Diagnostic setup.

The plasma density was measured with a 0.1 mm diam, 2 mm-long cylindrical probe biased −50 V with respect to ground. In addition, the angular distribution of the ion flux from the thruster was measured using a 25 mm diameter planar guarding sleeve probe. The plume probe was placed at the distance of 700 mm from the channel exit and rotated ±90° relative to the thruster axis.[23] The plume probe was biased −30 V with respect to ground.

The floating potential measurements were conducted first without the heating (cold probe) and then with heating (emissive probe). The probe heating was gradually increased during several probe insertions until the floating potential clearly saturated along the travel path of the probe. Measurements with cold and saturated emissive probe were repeated several times in each operating regime. All the probe potentials and the discharge current were monitored and recorded by a PC control and data acquisition system. Overall, the standard deviation of the floating probe measurements was in the range of ±5–15%.

B. Determination of plasma parameters

A detailed procedure for determination of the plasma parameters from the floating potential measurements is described in our previous publications[15,16,24] and in Appendix A. Essentially, we ascribed the change in the emissive probe potential as due to the effect of space charge limited electron emission, under the assumption that the plasma electrons are Maxwellian. The plasma potential, ϕ_{pl}, and the electron temperature, T_e, are obtained from the measured floating potentials of the emissive and cold probes using Eqs. (A6) and (A7). Although a procedure using nonbiased probes in Hall thrusters is clearly advantageous, the assumption of the Maxwellian EDF may introduce an uncertainty in the determination of the electron temperature. However, a comparison with other probe techniques[16,21,24] suggests that Eq. (A7) does give an approximate value of the mean electron energy in the thruster plasma.

Another uncertainty in the determination of the electron temperature stems from the fact that, in order for the unmagnetized probe theory to be valid,[25] it is necessary to keep the probe wire diameter much smaller than the electron gyrodiameter. For Hall thrusters, this makes the wire diameter comparable with the plasma Debye length and, therefore, the floating probe may collect charge carriers in the orbital mo-

Downloaded 18 Jul 2005 to 198.35.4.202. Redistribution subject to AIP license or copyright, see http://pop.aip.org/pop/copyright.jsp

tion limited (OML) regime. The analysis of this uncertainty is given in Appendix A. The maximum possible deviation of the true electron temperature from the one calculated according to the procedure described above is ±17%. Note that, for a smaller Hall thruster, the discrepancies between the values of ϕ_{pl} and T_e determined from the V-I characteristics of a biased planar probe ($a/\lambda_d \gg 1$) and from the above procedure for a floating 0.1 mm diameter cylindrical probe were less than 10% and 16%, respectively.[24] In the experiments described here, the ratio a/λ_d was smaller than that in Ref. 24.

The plasma density along the channel median was obtained from the measurements of the ion current collected by the movable biased probe. The OML approximation [Eq. (A3)] was used to interpret the data. The probe voltage with respect to the surrounding plasma was calculated from the measured plasma potential distribution. Note that Eq. (A3) determines the maximum ion current that can be collected by a cylindrical probe with a given collection area. Therefore, the value of the plasma density obtained from this equation is likely to give the upper bound of the possible (true) plasma density. In addition, the plasma density distribution was deduced from the plume probe measurements. The total ion flux in the plume, I_{it}, was obtained by integrating the measured angular distribution of the ion current. Assuming a continuous one-dimensional axial flow of monoenergetic ions with velocity $v_i(z)=[2e(\phi^a_{\mathrm{pl}}-\phi_{\mathrm{pl}}(z))/M]^{0.5}$, one can get the plasma density distribution along the channel median from the total ion flux as $N_i(z)=I_{\mathrm{it}}/ev_i(z)A(z)$. Here N_i is the ion density, ϕ^a_{pl} is the plasma potential at the anode side, and $A(z)$ is the cross-section area of the ion beam. $A(z)$ was estimated assuming the beam divergence half-angle to be constant along z. The values of the divergence half-angle were deduced from plume measurements using the procedure of Ref. 23. In these experiments, the half-angle was in the range of 50°–57° in the discharge voltage range of 200–700 V. Since there are presumably no significant particle sinks or sources in the plasma plume, such estimation of the plasma density gives an approximate lower bound of the true plasma density near the channel exit.

C. Thruster operational procedure

At the beginning of each set of probe measurements, in order to reach a steady-state the thruster was continuously operated at the discharge voltage of 200–300 V for approximately 1–2 hours. The steady-state was monitored by measuring the discharge current. Then the discharge voltage was changed to the desired operating level and the probe measurements were performed. When increasing the voltage to 400 V and higher, we encountered two steady-state regimes of the thruster, one of which appears to be transitional. The transitional regime occurs after the discharge current initially increases to a high value and then saturates at this value for a few tens of minutes. After that the discharge current slowly reduces to a smaller value, which corresponds to the second steady-state regime. The duration of this transition was usually longer for higher discharge voltages and could take between 30 minutes and about an hour. In the present work we discuss experimental results obtained mainly in the transitional regime, but a comparison of key results for both steady-state regimes is given in Appendix B. It appears that the main conclusions of this paper on the role of SEE in high discharge voltage thruster operation are valid for both steady-state regimes.

III. EXPERIMENTAL RESULTS

Figure 3 shows the voltage-current characteristic of the thruster. Results of the plasma measurements are shown in Fig. 4. A significant voltage potential drop is localized in the region with a strong radial component of the magnetic field. This region is usually referred to as the acceleration region. The voltage drop in the acceleration region is 80–90% of the applied discharge voltage, V_d. The electron temperature has a local maximum in the acceleration region.

Figure 5 shows how the maximum electron temperature depends on the discharge voltage. The discharge voltage threshold, $V_d \sim 400$ V, separates two temperature regimes: (i) below the voltage threshold $T_{e\,\max}$ increases almost linearly with the discharge voltage and (ii) in the range $400\ \mathrm{V} < V_d < 600$ V, the electron temperature saturates at about 50–60 eV. Some increase of $T_{e\,\max}$ is also observed at $V_d > 550$–600 V, which may manifest a transition to the third temperature regime. According to the plume measurements, the increase of the discharge current at $V_d > 400$ V is due primarily to the increase of the electron current.

In general, these experimental results appear to agree with the theoretical predictions of Barral *et al.*[9] and Ahedo *et al.*[10,11] The transient fluid model[9] assumes the cathode plane to be located at the channel exit and includes the effective anisotropy of the electron temperature. Alternatively, Ahedo *et al.* consider the near-field plume region and use exact solutions from the radial model. The magnetic field in this fluid model[10,11] increases with the discharge voltage in order to maximize the thruster efficiency. In spite of these different approaches, both models[9–11] predict the same trends in the dependence of the electron temperature on the discharge voltage. They predict three regimes separated by two discharge voltage thresholds: below the first voltage threshold, which is less than or equal to about 200–250 V, SEE does not significantly affect the electron temperature and $T_{e\,\max}$ grows with V_d. At $V_d > 400$–450 V the near-wall sheaths appear to be space charge saturated due to strong SEE, and $T_{e\,\max}$ grows with V_d again. The intermediate regime between the two voltage thresholds is characterized by the temperature saturation due to the electron energy loss at the walls, which is enhanced by SEE. In Fig. 5 we attempted to identify these three regimes for the experimental dependence of $T_{e\,\max}$ on V_d.

The linear dependence of the local T_e on the local ϕ_{pl} at $V_d < 400$ V shown in Fig. 6(a), supports the prediction[9–11] that there are no SEE effects below the first discharge voltage threshold. The electron energy gain $dT_e/d\phi_{\mathrm{pl}}$ is nearly constant, ~0.15, both inside and outside the channel exit. It is worth mentioning that although the existence of a constant electron energy gain, which was first reported by Staack *et al.*,[15] is not predicted by the fluid models, the linear relationship between the macroscopic parameters $T_{e\,\max}$ and V_d was

Downloaded 18 Jul 2005 to 198.35.4.202. Redistribution subject to AIP license or copyright, see http://pop.aip.org/pop/copyright.jsp

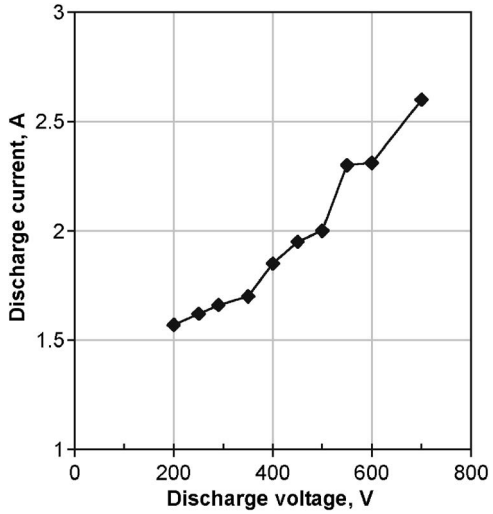

FIG. 3. Current vs voltage characteristic of the Hall thruster measured for xenon flow of 19 sccm and a constant magnetic field.

also found in simulations of Ahedo *et al.*[11] Kim[26] also reported earlier $T_{e\,\max} \approx (0.07-0.09)eV_d$ for the state-of-the-art Russian Hall thrusters.

Above the discharge voltage threshold the local temperature maximum shifts outside the channel exit [Figs. 4 and 6(b)]. In the temperature saturation regime, $400\ \mathrm{V} < V_d < 600\ \mathrm{V}$, a fraction of the voltage drop between the location of $T_{e\,\max}$ and the cathode side of the acceleration region remains almost constant and approximately equal to 300 V. According to the model,[10] the outward shift of $T_{e\,\max}$ occurs as the energy loss at the walls exceeds the Joule heating in the channel with SCS wall sheaths. Interestingly, in the experiments with a narrow thruster channel, which we described in Ref. 16, the local temperature maximum remained in the near-field plasma plume as the discharge voltage was increased from 150 to 500 V, while the temperature saturation still occurred above the voltage threshold of about 400 V. An enhancement of the electron mobility inside the narrow channel was suggested by a hydrodynamic model[16] as an explanation to the outward shift of the acceleration region, and the local maximum of the electron temperature. Therefore, the outward shift of the local temperature maximum, which is shown here for the temperature saturation regime, may not necessarily result from the enhancement of electron energy losses at the channel.

It is important to emphasize that the models[9–11] considered the types of boron nitride ceramic material that have lower SEE yield than grade HP boron nitride, which was used in our experiments. For the "low SEE" materials used in the modeling, the effective SEE coefficient δ, averaged over the Maxwellian EDF, approaches the critical value $\delta_c \lesssim 1$ at $T_e \sim 30-40$ eV.[9–11] Therefore, according to these models, $T_{e\,\max}$ in the temperature saturation regime is also equal to 30–40 eV. For grade HP boron nitride the critical SEE is achieved at $T_e^* \approx 18$ eV,[17,18] while the measured $T_{e\,\max}$ is two to three times larger than T_e^*. The transition to the temperature saturation occurs at the discharge voltage almost

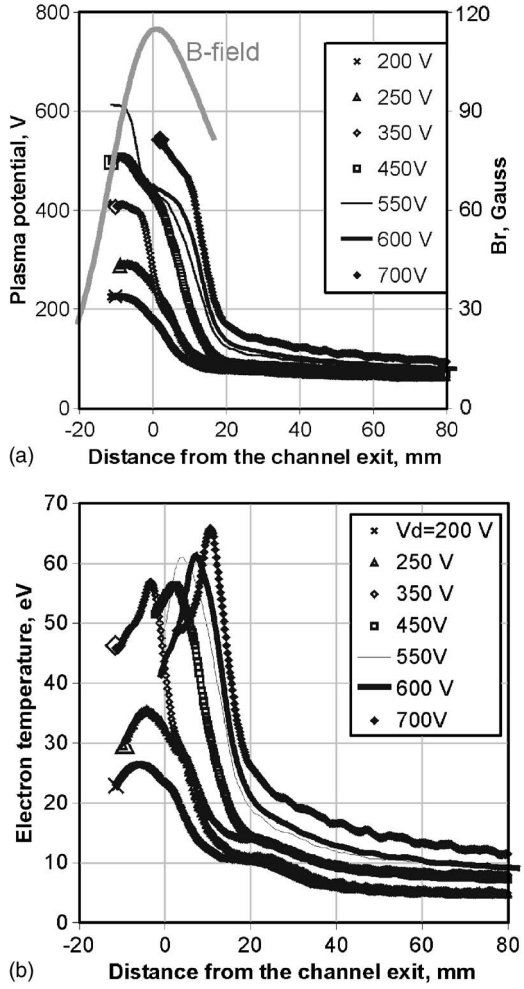

FIG. 4. Distributions of the plasma potential (a) and the electron temperature (b) measured along the channel median. The anode position is –46 mm relative to the channel exit. The radial magnetic field profile corresponds to the operating conditions.

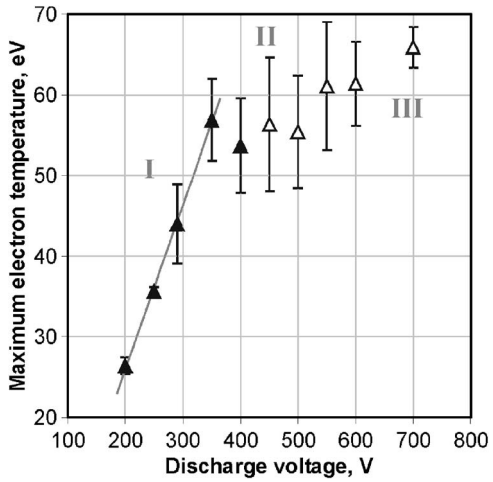

FIG. 5. Experimental dependence of the maximum electron temperature on the discharge voltage. Empty triangles correspond to the maximum electron temperature located outside the channel exit. I, II, and III are the temperature regimes, which appear to be qualitatively similar to the regimes predicted by the models (Refs. 9–11). The error bars show the standard deviations obtained from several probe insertions.

Downloaded 18 Jul 2005 to 198.35.4.202. Redistribution subject to AIP license or copyright, see http://pop.aip.org/pop/copyright.jsp

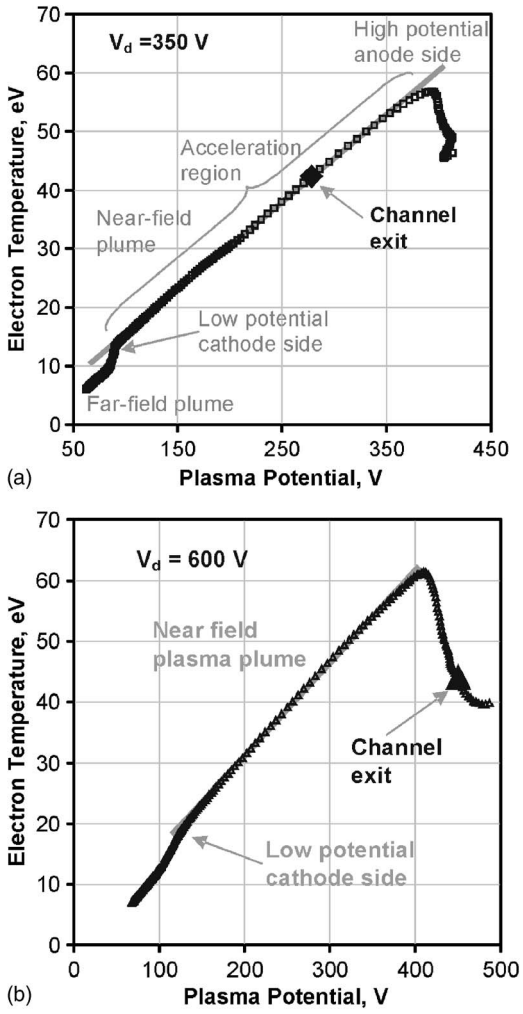

FIG. 6. Local electron temperature versus local plasma potential measured along the channel median for the discharge voltage of 350 V (a) and 600 V (b). Electron energy gain $dT_e/d\phi_{\mathrm{pl}}$ in the regions with linear variations of the electron temperature with the plasma potential are ~0.15 for 350 V and ~0.16 for 600 V.

twice larger than that predicted by the model of Ahedo *et al.*[10,11]

IV. DISCUSSION

A. On the possibility of space charge saturated sheath regime

The electron energy loss at the walls can be used to calculate the effective electron-wall collision frequency. We consider only (i) the electron temperature saturation regime ($V_d > 400$ V) and (ii) the region just outside of the channel exit, where the electron temperature has a local maximum. The model[10,11] predicts that this maximum is likely to appear due to the balance of the Joule electron heating and electron energy losses to the channel walls. The 1-D electron energy balance equation in this model reads[10]

$$\frac{1}{A}\frac{d}{dz}\left[\frac{5}{2}T_e\Gamma_e + A\left(-\frac{5}{2}\frac{\nu_e N_e T_e}{\omega_{ce}^2 m_e}\frac{dT_e}{dz}\right)\right] = eN_eV_e\frac{d\phi}{dz} - N_e(\nu_w\varepsilon_w + \nu_i\varepsilon_i). \tag{1}$$

Here, A is the cross section of the ion flux, ν_w is the electron-wall collision frequency, Γ_e is the electron flux across the radial magnetic field, and ε_w is the energy loss at the wall per one electron; ν_i and ε_i are the ionization frequency and energy loss per one ionizing collision, respectively. Let us denote the location of the $T_{e\,\max}$ as $z^*: dT_e/dz(z^*)=0$. Simplifying Eq. (1) at $z=z^*$, we obtain

$$\nu_w\varepsilon_w = eV_e\frac{d\phi}{dz} - \left[\nu_i\varepsilon_i + \frac{5}{2}\frac{T_e}{N_eA}\frac{d\Gamma_e}{dz} - \frac{5}{2}\frac{\nu_e T_e}{\omega_{ce}^2 m_e}\frac{d^2T_e}{dz^2}\right]. \tag{2}$$

This equation allows one to estimate the maximum possible electron-wall collision frequency. The term in the brackets in the right-hand side of Eq. (2) represents the combined effect of the heat conduction and the energy losses for ionization. This term is positive near $z=z^*$ under typical operating conditions. Thus, the maximum electron-wall collision frequency is obtained by equating the electron energy loss at the walls and Joule heating P_J

$$\nu_w\varepsilon_w = P_J = \frac{I_e}{AN_e}\frac{d\phi}{dz}, \tag{3}$$

where $I_e(z)=I_d-I_i(z)$ is the cross-field electron current and I_d is the discharge current.

In the commonly accepted model of electron-wall interaction, the electron energy loss at the walls for the Maxwellian electrons can be expressed as[8,9]

$$\nu_w\varepsilon_w = \frac{\tilde{\nu}}{h}\sqrt{\frac{T_e}{M_i}}\frac{1}{1-\delta}[2T_e + (1-\delta)e|\phi_w|], \tag{4}$$

where $\tilde{\nu}\sim 0.7-1.2$ for typical thruster conditions,[10] h is the channel width, δ is the SEE coefficient of the channel walls, and ϕ_w is the potential drop between the plasma and the wall. It is instructive to compare two opposite limiting cases: SCS regime with $\delta\approx\delta_c$ and the regime with no SEE ($\delta \ll 1$). In the SCS regime, the electron energy removed from the plasma is $2T_e+(1-\delta)e|\phi_w|$, and the theoretical electron-wall collision frequency is

$$\nu_{\mathrm{th}}^{\mathrm{SCS}} \approx \frac{1}{h}\sqrt{\frac{T_e}{M_i}}\frac{1}{1-\delta_c}, \tag{5}$$

where $\delta_c\approx 0.983$ for xenon plasma. Here we assumed $\tilde{\nu}\approx 1$. Hence, we can obtain the experimental electron-wall collision frequency as

$$\nu_{\mathrm{exp}}^{\mathrm{SCS}} \approx \frac{P_J}{2T_e}. \tag{6}$$

In the regime without SEE, the theoretical electron-wall collision frequency is equal to the wall recombination frequency

Downloaded 18 Jul 2005 to 198.35.4.202. Redistribution subject to AIP license or copyright, see http://pop.aip.org/pop/copyright.jsp

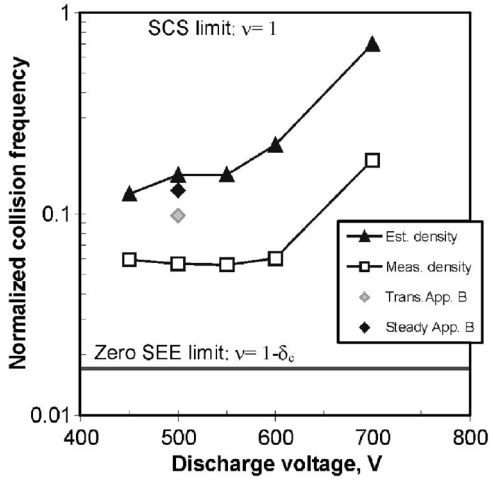

FIG. 7. The experimentally obtained electron-wall collision frequencies $\nu_{\mathrm{exp}}^{\mathrm{SCS}}$ [Eq. (6)] normalized to $\nu_{\mathrm{th}}^{\mathrm{SCS}}$ [Eq. (5)]. For each discharge voltage, the experimental frequencies are given for the measured and estimated values of the plasma density. The regimes with SCS sheaths and zero SEE correspond to the straight lines $\nu=1$ and $\nu=(1-\delta_c)\approx 0.017$, respectively. In addition, the experimental frequencies for transitional ◆ and steady-state regimes ◆ from Appendix B are shown.

$$\nu_{\mathrm{th}}^{0} \approx \frac{1}{h}\sqrt{\frac{T_e}{M_i}}, \tag{7}$$

while the energy carried by an electron to the wall is rather difficult to quantify, because it depends on the shape of the electron distribution function, in particular, on the effective temperature of the tail and bulk electrons and anisotropic properties.[27] We note that for Maxwellian electron EDF and xenon plasma, $\varepsilon_w \approx 7.77 T_e$ and the experimental electron-wall collision frequency is $\nu_{\mathrm{exp}}^{0} \approx P_j / 7.77 T_e$.

To compare the experimental and theoretical values of the electron-wall collision frequency, in Fig. 7 we plot $\nu_{\mathrm{exp}}^{\mathrm{SCS}}$ [Eq. (6)] normalized to $\nu_{\mathrm{th}}^{\mathrm{SCS}}$ [Eq. (5)]. The two limiting regimes are represented by the straight lines in Fig. 7. The SCS regime corresponds to the normalized frequency $\nu=1$, and the regime with zero SEE is shown by $\nu=\nu_{\mathrm{th}}^{0}/\nu_{\mathrm{th}}^{\mathrm{SCS}}=(1-\delta_c)$. For each discharge voltage, the experimental frequencies are given for the measured and estimated values of the plasma density. In calculations of $\nu_{\mathrm{th}}^{\mathrm{SCS}}$ we assumed that electrons are bouncing along the magnetic field lines and also took into account that the local maximum T_e is outside the channel exit. Therefore, in Eq. (5), h was taken roughly as the distance measured along the magnetic field line passing through z^* [see Figs. 1 and 4(b)] between the intersections of this field line with the thruster end walls. The electric field was obtained by numerically differentiating the measured plasma potential distributions.

We note that under the assumption of the space charge saturated sheath, the frequency ratio is below unity for all discharge voltages (Fig. 7). The value of the collision frequency obtained from the experiment approaches the theoretical value only at $V_d=700$ V. The estimated plasma density $\sim 5\times 10^{10}\ \mathrm{cm}^{-3}$, is almost twice smaller than the measured density and gives a better agreement of experimental collision frequency with the theoretical value. In the temperature saturation regime ($400\ \mathrm{V} < V_d < 600\ \mathrm{V}$) the experimental frequency is more than an order of magnitude lower than the theoretical SCS limit. Therefore, the SCS regime of the wall sheaths is unlikely realized even at such high electron temperature, $T_e \sim 55-60$ eV, as measured in this voltage range.

The discrepancy between $\nu_{\mathrm{exp}}^{\mathrm{SCS}}$ and $\nu_{\mathrm{th}}^{\mathrm{SCS}}$ can be reduced due to two effects that are rather difficult to quantify accurately. First, energy re-injection into the plasma by the backscattered electrons can slightly increase the value of $\nu_{\mathrm{exp}}^{\mathrm{SCS}}$. For the Maxwellian EDF, the right-hand side of Eq. (6) should be, in fact, divided by factor $1-\eta\tau$, where η and τ are the average backscattering yield and the backscattered energy fraction, respectively. Although the exact values of η and τ are unknown, both of them can be taken on the order of 0.5.[9] Thus, the estimated increase of $\nu_{\mathrm{exp}}^{\mathrm{SCS}}$ due to electron backscattering can be about 35%. Second, the real values of $\nu_{\mathrm{th}}^{\mathrm{SCS}}$ can be smaller that those determined from Eq. (5), if the EDF is substantially anisotropic, with a lower electron temperature along the magnetic field lines. In this case, the electron temperature in Eq. (5) should be replaced with $T_{e\|}$. As stated herein, investigation of the EDF anisotropy was outside of the scope of the present study. The numerical simulations by Barral *et al.* suggest that the temperature anisotropy with $T_{e\perp}/T_{e\|}\sim 3$ could occur under certain conditions.[9] If such EDF anisotropy was, in fact, realized in our experiments, it would make the values of $\nu_{\mathrm{th}}^{\mathrm{SCS}}$ somewhat smaller than those calculated from Eq. (5). However, in the discharge voltage range from 400 to 600 V, $\nu_{\mathrm{th}}^{\mathrm{SCS}}$ would remain much larger than $\nu_{\mathrm{exp}}^{\mathrm{SCS}}$.

If we assume that SEE from the walls is weak and electrons are Maxwellian, we can estimate the ratio of the experimental electron-wall collision frequency to the theoretical frequency in the regime without SEE [Eq. (7)], $\nu_{\mathrm{exp}}^{0}/\nu_{\mathrm{th}}^{0}$. For the discharge voltage of 700 V, the experimental frequency is about an order of magnitude higher than the theoretical frequency in the regime without SEE. In the discharge voltage range of 450–600 V, $\nu_{\mathrm{exp}}^{0}/\nu_{\mathrm{th}}^{0}\sim 0.9$ for measured plasma densities and $\sim 2-3$ for estimated plasma densities. However, it is unclear what physical mechanisms could keep SEE low when the electron temperature is so high. A truncation of the electron EDF at high energy is known to affect the sheath potential drop.[28] A kinetic study of electron dynamics in Hall thrusters showed that the temperature of tail electrons is 2–3 times smaller than the temperature of the bulk electrons.[17] In this case, the electron energy removed from the plasma due to wall losses is smaller than $7.77\ T_e$. Taking into account this effect in the above estimations should lead to larger values of the experimental electron collision frequency in the regime without SEE.

It is important to mention here that the measured ratio of the total outgoing ion flux to the input flux of neutral gas atoms (the thruster propellant utilization) was in the range 0.8–0.9, which is typical for the state-of-the-art Hall thrusters.[29,30] The presence of slow charge-exchange ions in the plume and multicharged ions from the thruster[30] could still lead to the overestimation of the plasma density. However, an ~70% reduction of the total ion flux is required for the experimental frequency to match the theoretical SCS limit at, for instance, $V_d=550$ V.

Downloaded 18 Jul 2005 to 198.35.4.202. Redistribution subject to AIP license or copyright, see http://pop.aip.org/pop/copyright.jsp

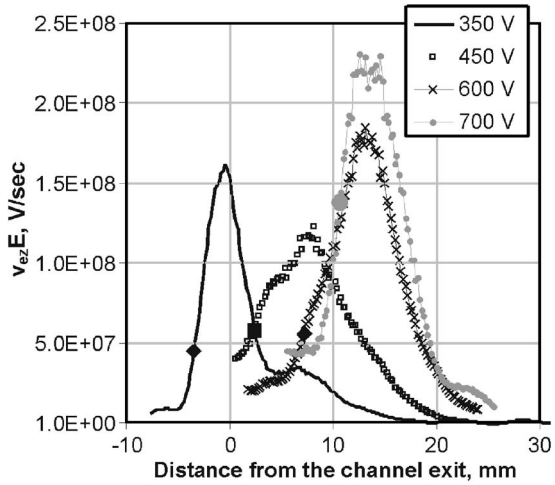

FIG. 8. Joule heating profile along the channel median for different discharge voltages. Enlarged markers correspond to the location of the maximum electron temperature. The anode position is −46 mm relative to the channel exit.

B. Temperature saturation regime

In this section we discuss the physical mechanisms that can possibly cause the observed saturation of the maximum electron temperature. In Fig. 8 we plot the Joule heating per one electron P_J. It is evident that the Joule heating reduces towards the thruster exit starting from some location $z' > z^*$. The experimental data inside the channel are subjected to the probe-induced perturbations and therefore is not considered here. The reduction of the Joule heating is due to the decrease of the electric field (see Fig. 4) which, in its turn, occurs probably because of a local increase of the electron cross-field mobility. The growth of the electron cross-field mobility might explain also the observed saturation of the voltage drop in the part of the acceleration region outside the channel exit. As a result of the reduced electric field, the Joule heating in the near-field plume is, most likely, not as large as in the models.[9–11] In order to balance the Joule heating at z^*, the electron energy loss at the walls does not have to be enhanced due to SCS sheaths. An electron cooling, which occurs between z^* and the channel exit, brings the electron temperature to the values lower than the maximum electron temperature measured inside the channel in the regimes without SEE effects ($V_d < 350$ V in Fig. 4).

We note that Barral *et al.* predict an increase of the electron mobility due to the near-wall conductivity, which requires a significant SEE to enhance electron collisions with the walls. The latter is not evident from the analysis of the experimental wall collision frequency. Ahedo *et al.* increase the magnetic field strength with the discharge voltage and, thus, effectively control the electron transport which, in their case, is dominated by anomalous Bohm-type diffusion. Therefore, in spite of the qualitative similarities between the experimental and theoretical results, the physical mechanisms, which cause the observed temperature saturation, might be either different than those suggested by the theory or involve kinetic (possibly, nonstationary[31]) regimes of the electron-wall interaction, which can be captured neither by the averaged measurements of the present work nor by the fluid models.

Finally, other mechanisms of electron energy losses might make, in principle, a significant contribution to the overall energy balance. One such mechanism is the electron energy loss due to ionization and excitation of neutral atoms. We can estimate the neutral gas density that would be sufficient to balance the Joule heating with the electron energy losses due to inelastic electron-atom collisions at z^*. Neglecting the wall energy losses and heat conduction in Eq. (2), for $V_d = 450-550$ V and 19 sccm xenon flow we get the required neutral density to be about $1-3\times10^{12}$ cm^{-3}, which is not unreasonable.

C. On the constant electron energy gain

Figure 6(a) shows that below the discharge voltage threshold roughly similar energy gain is obtained in the acceleration region and in the far-field plasma plume of the Hall thruster. Above the voltage threshold [Fig. 5(b)], the constant energy gain holds also in the far-field plume and in part of the near-field plume for $T_e < T_{e\,\max}$. In the far-field plume, where the magnetic field $B \approx 0$, the plasma jet expands freely. In this case expansion of the electron component can be described by the fluid momentum equation

$$\nabla(N_e T_e) = eN_e \nabla \phi. \tag{8}$$

In plasma expansion problems it is customary to use the polytropic equation of state,[32]

$$T_e/N_e^{\gamma-1} = \text{const}, \tag{9}$$

where γ is the polytropic index. This approach is widely used for plasma plume modeling in Hall thrusters.[33–35] From Eqs. (8) and (9) we find that the electron temperature is proportional to the plasma potential

$$\nabla T_e = \beta e \nabla \phi, \tag{10}$$

where $\beta = (\gamma-1)/\gamma$. This fact agrees with the results of the measurements. It is important to emphasize here that the effective polytropic index γ that corresponds to the measured coefficient $\beta \approx 0.13-0.15$, is $\gamma = (1-\beta)^{-1} \approx 1.15-1.18$. The notion of the effective polytropic exponent is used extensively in the problems of astrophysical, solar, and magnetospheric plasmas.[36–38] In our case, the effective γ falls quite reasonably between the limiting values that correspond to the isothermal ($\gamma=1$) and adiabatic approximations ($\gamma=5/3$). This implies that the electron heat conduction is neither zero nor infinite, but takes a finite value. Possibly it is controlled by some anomalous process such as, for instance, electron-wave scattering.[39]

We note that Eq. (10) holds also in the near-field thruster plume, where the strong radial magnetic field impedes the axial electron motion and Eq. (8) is inapplicable. The same dependence of T_e on ϕ with and without the magnetic field suggests that the physical mechanism that governs the electron temperature is likely to be independent of B. Therefore, one may speculate that the anomalous electron heat conduc-

Downloaded 18 Jul 2005 to 198.35.4.202. Redistribution subject to AIP license or copyright, see http://pop.aip.org/pop/copyright.jsp

tion is either independent of B, or determined by some nonlocal process that establishes the same heat conduction value over the entire Hall thruster plume.

V. CONCLUSIONS

Macroscopic effects of the wall energy losses and Joule heating on the electron temperature in a Hall thruster were analyzed using the measured plasma potential, electron temperature, and plasma density. We observed the discharge voltage threshold above which the maximum electron temperature saturates at about 50–60 eV. The analysis of the experimental electron-wall collision frequency suggests that this frequency is larger than wall recombination frequency and much smaller than the theoretical electron-wall collision frequency obtained for the space charge saturated sheath regime. Therefore, existing Hall thruster models cannot quantitatively explain the electron temperature saturation which is, according to our measurements, associated with a decrease of the Joule heating. In addition to electron energy losses at the walls, a possible energy loss mechanism balancing the Joule heating in the very near-field plasma plume includes energy losses due to inelastic electron-atom collisions.

The reduced sensitivity to the SEE indirectly supports recent kinetic studies, which suggest that the electron EDF is depleted at high energy due to electron-wall collisions. In this case, the effective secondary electron emission coefficient is lower than that for the Maxwellian EDF. The reduced SEE may also explain why the transition to the space charge saturated sheath regime can only occur at higher electron temperatures than those predicted by the fluid models. Space charge saturation of the wall sheaths might involve kinetic and nonstationary effects. It is important to mention that the study of these effects is outside of the scope of the present work, limited to the measurements of the averaged plasma parameters.

Below the discharge voltage threshold we further demonstrated a linear relationship between the local electron temperature and the local plasma potential in the acceleration region both inside and outside the channel exit. Here, we showed that the linear dependence also holds in the far-field plume, as well as in the regimes above the discharge voltage threshold between the local maximum of the electron temperature and the cathode side of the acceleration region. The mechanisms governing the electron temperature in the acceleration region may be independent of the magnetic field or nonlocal processes.

The important implications of this work include: (1) that the theoretical modeling and experimental studies of thruster processes need to focus more on kinetic and nonstationary effects; and (2) that, in light of the effects on the electron temperature, by adjusting voltages,[40,41] channel geometry,[16] or wall material properties,[42] further optimizations are possible in reaching higher efficiency in the Hall thruster.

ACKNOWLEDGMENTS

The authors wish to thank Dr. Leonid Dorf for his help with experiments and useful discussions and comments on this paper. The authors benefited from discussions with Professor Amnon Fruchtman, Dr. Igor Kaganovich, Dr. Michael Keidar, and Dr. Alexander Dunaevsky.

This work was supported by U.S. DOE Contract No. AC02-76CH0-3073.

APPENDIX A: UNCERTANITIES IN PROBE MEASUREMENTS

The method of determining the electron temperature T_e from the floating potentials of the cold and hot cylindrical emissive probe relies on our knowledge of the electron and ion currents drawn by the probe at a given potential. In general, the floating potential of a probe adjusts itself so that the probe draws no net current in a steady-state. Thus, the floating probe retards the incident electrons and attracts the ions. In the case of the retarding potential, the electron current to the cylindrical probe is well-known and given by[43]

$$I_e(V) = \frac{eN_eA_p}{4}\sqrt{\frac{8T_e}{\pi m}}\exp\left(\frac{eV}{T_e}\right), \tag{A1}$$

where V is the probe potential with respect to the surrounding plasma, N_e is the electron density in the unperturbed plasma, A_p is the probe collection area, and m is the electron mass. This current is completely independent of the sheath size, which is not the case for the ion current to the attracting probe. In general, the current of charge curriers to the attracting probe depends on the ratio a/λ_D, where a is the probe radius and λ_D is the plasma Debye length.[43,44]

For the probe radius large with respect to the Debye length ($a \gg \lambda_D$), we are in the well-known thin (planar) sheath limit, which requires that ions be accelerated to the Bohm velocity before entering the sheath.[45–47] In this case all ions entering the sheath are collected by the probe and, equating the ion and electron fluxes, we obtain the floating potential of a cold probe:

$$\phi_{\mathrm{fl}}^{\mathrm{cold}} = \phi_{\mathrm{pl}} + T_e \ln\left(0.61\sqrt{\frac{2\pi m}{M}}\right) \approx \phi_{\mathrm{pl}} - 5.77T_e, \tag{A2}$$

where M is the mass of a xenon atom. In the opposite limiting case of a thick sheath ($a \ll \lambda_D$), the simple analytical expressions exist if the potential around the probe decreases more slowly than r^{-2}. Under these assumptions, we are in the orbital motion limited (OML) regime.[48] In this regime, for every ion energy there exists an impact parameter that makes the ion hit the probe with a grazing incidence. The maximum impact parameter for hitting the probe is then a simple function of the ion initial energy and the probe potential. The ion current to the probe is given in this case by

$$I_i(V) = \frac{2eN_iA_p}{\sqrt{\pi}}\sqrt{\frac{-eV}{2\pi M}}. \tag{A3}$$

It is important to emphasize that the OML current is the maximum ion current that can be collected by a cylindrical probe with a given collection area. Then, by equating the electron and ion currents, we find that the floating probe potential satisfies in this case the equation

Downloaded 18 Jul 2005 to 198.35.4.202. Redistribution subject to AIP license or copyright, see http://pop.aip.org/pop/copyright.jsp

$$\frac{4m}{\pi M} = \frac{-\exp(2\phi)}{\phi}, \tag{A4}$$

where $\phi = \phi_{\mathrm{fl}}^{\mathrm{cold}} - \phi_{\mathrm{pl}}$. The numerical solution of this equation for xenon plasma is

$$\phi_{\mathrm{fl}}^{\mathrm{cold}} = \phi_{\mathrm{pl}} - 5.24T_e. \tag{A5}$$

Thus, we observe that the absolute value of the floating potential in the thick sheath case is about 10% smaller than that in the thin sheath case. The floating potential shifts closer to the plasma potential.

As the ratio a/λ_D increases and becomes $a/\lambda_D \sim 1$, the OML theory breaks down. This happens because of specific potential distribution around the probe which can reflect ions that would not be reflected in the simpler, e.g., Coulomb-like potential. The case of arbitrary ratio a/λ_D is very complex and can be treated only numerically. The corresponding problem was formulated and studied by Bernstein and Rabinowitz[49] and Laframboise.[50] The numerical results[50] were later fitted with rather simple analytical expressions by Steinbrüchel.[51] According to Steinbrüchel, the OML current (A3) remains a very good approximation to the numerical results for $a/\lambda_D \lesssim 3$. We notice, however, that for arbitrary a/λ_D the value of the floating potential of a cold probe lies between the upper and the lower bounds given by Eqs. (A5) and (A2), respectively.

In the case of the emissive probe, simple analytical expressions for the floating potential do not exist even in the planar model. Numerical solutions for the experimental conditions $T_e \gg T_i$, T_s (here, T_s is the temperature of the emitted electrons) were obtained by Schwager.[2] It was shown that the in the case $a \gg \lambda_D$ the floating potential saturates at

$$\phi_{\mathrm{fl}}^{\mathrm{em}} \approx \phi_{\mathrm{pl}} - 1.5T_e, \tag{A6}$$

with respect to the plasma potential. It is physically obvious that in the case of the emissive probe, similarly to the cold probe case, the floating probe potential shifts closer to the plasma potential as the sheath becomes thicker. However, the change of the floating potential may be smaller in this case, because the collected electron current is compensated primarily by the current of the emitted electrons, not by the ion current as in the cold probe case. Anyway, there are no readily available formula for calculation of the emissive probe floating potential in the thick sheath case.

For the typical HT plasma parameters $N_e \sim 5 \times 10^{11}$ cm^{-3} and $T_e \sim 20$ eV, the Debye length is about $\lambda_D \sim 0.05$ mm. The hotter or less dense the plasma is, the larger the Debye length is. If the emissive probe diameter is ~ 0.1 mm, $a/\lambda_D \sim 1$, and the planar probe approximation does not apply. In fact, according to Steinbrüchel, the OML theory is more appropriate to calculate the ion current and the floating potential. In the following, we estimate the maximum uncertainty which is introduced in the value of T_e when one uses the planar probe model to determine T_e from the measured floating potentials of the cold and hot cylindrical emissive probe. In the planar probe model, the electron temperature can be found from Eqs. (A2) and (A6):

$$T_e^{\mathrm{exp}} = \frac{\phi_{\mathrm{fl}}^{\mathrm{em}} - \phi_{\mathrm{fl}}^{\mathrm{cold}}}{4.27}. \tag{A7}$$

We denote this temperature T_e^{exp} to distinguish it from the true value of the electron temperature T_e. Now, the real T_e should be determined from the appropriate formula for the cylindrical probe. For the cold probe in the case $a \sim \lambda_D$ we can use Eq. (A5), while for the hot emissive probe we write

$$\phi_{\mathrm{fl}}^{\mathrm{em}} \approx \phi_{\mathrm{pl}} - \alpha T_e. \tag{A8}$$

Here, coefficient α is larger than zero, because the floating potential of the emissive probe should be less than the plasma potential. On the other hand, as follows from the comparison with the thin sheath case, $\alpha < 1.5$. Thus, we obtain

$$T_e = \frac{\phi_{\mathrm{fl}}^{\mathrm{em}} - \phi_{\mathrm{fl}}^{\mathrm{cold}}}{5.24 - \alpha} = \frac{4.27T_e^{\mathrm{exp}}}{5.24 - \alpha}. \tag{A9}$$

The minimal possible value of T_e is $T_e(\alpha = 0) = 0.815T_e^{\mathrm{exp}}$, whereas the maximum value of T_e is $T_e(\alpha = 1.5) = 1.142T_e^{\mathrm{exp}}$. Therefore, the gross formula for the uncertainty of the electron temperature is

$$\Delta T_e \approx \pm 0.17T_e^{\mathrm{exp}}. \tag{A10}$$

This formula gives the maximum possible deviation of the real electron temperature from the one calculated in the planar probe model.

APPENDIX B: TRANSITIONAL AND STEADY-STATE OPERATING REGIMES

The thruster operation at high discharge voltages usually exhibits a long transitional operation, which precedes a steady-state operation. During the transitional operation, the discharge current is always larger than the steady-state value. A similar behavior was first observed by Hofer *et al.*[52] for a different Hall thruster. Morozov *et al.*[53] showed how a coating of the channel walls with sputtered materials from the vacuum vessel walls might affect the discharge current and, in particular, the time needed to reach a steady-state. For high discharge voltages, this sputtering by energetic ions from the thruster is an issue. The coating of the thruster channel may result in changes of SEE properties of the channel walls. Therefore, it is actually not clear which of these operating regimes is more affected by sputtering effects in laboratory environments.

Figure 9 shows the dependence of the local electron temperature on the local plasma potential measured for the transitional and steady-state operations at the same discharge voltage of 500 V. The magnetic field was similar to the one used in our previous study.[16] It was different from the magnetic field distribution shown in Fig. 1. The channel width was 25 mm. A quasi-steady-state value of the discharge current during the transitional operation was 1.97 A, while in the "true" steady state it was 1.63 A. For both operating regimes, the saturation of the maximum electron temperature was observed above the discharge voltage threshold of 400 V. The saturation temperature was approximately $\sim 50-60$ eV (Fig. 9). For the steady-state operation, the

Downloaded 18 Jul 2005 to 198.35.4.202. Redistribution subject to AIP license or copyright, see http://pop.aip.org/pop/copyright.jsp

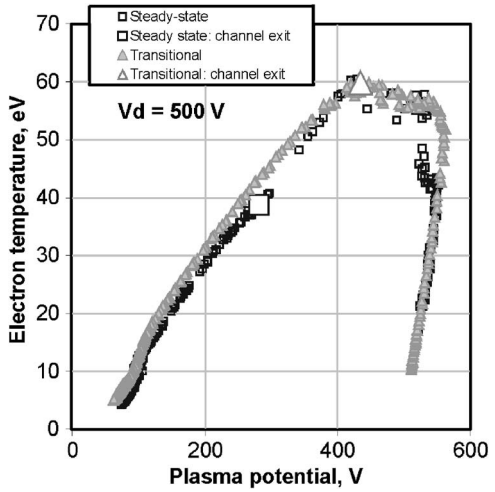

FIG. 9. Local electron temperature vs local plasma potential measured along the channel median for the discharge voltage of 500 V for transitional and steady-state operation. The thruster operation: xenon gas flow 19 sccm, the magnetic field distribution of Ref. 16. The enlarge markers correspond to the local parameters at the channel exit.

maximum electron temperature is located inside the channel. A linear dependence of the local electron temperature on the local potential is seen inside the channel as well.[16] For the transitional operation, the local electron temperature peaks outside the channel similarly to the results shown in Fig. 6. Figure 7 shows that the experimental frequencies obtained for the estimated values of the plasma density are still below the theoretical frequency for the SCS sheath (Fig. 7). Thus, despite the differences in the distributions of the local parameters, for both operating regimes the electron energy loss at the walls does not have to be enhanced due to SCS sheaths in order to balance the Joule heating.

[1] G. D. Hobbs and J. A. Wesson, Plasma Phys. **9**, 85 (1967).
[2] L. A. Schwager, Phys. Fluids B **5**, 631 (1993).
[3] T. Intrator, M. H. Cho, E. Y. Wang, N. Hershkowitz, D. Diebold, and J. DeKock, J. Appl. Phys. **64**, 2927 (1988).
[4] G. F. Mattews, G. M. McCracken, P. Swell, M. Woods, and B. J. Hopkins, J. Nucl. Mater. **145–147**, 225 (1987).
[5] N. Ohyabu, J. Nucl. Mater. **196–198**, 276 (1992).
[6] P. C. Stangeby, in *The Plasma Boundary of Magnetic Fusion Devices*, Plasma Physics Series (IOP, Bristol, 2000), pp. 646–654.
[7] R. Chodura, in *Physics of Plasma-Wall Interaction in Controlled Fusion*, NATO Advanced Science Series, edited by D. E. Post and R. Behrisch (Plenum, New York, 1986), p. 99; P. Stangeby, *ibid.*, p. 41.
[8] M. Keidar, I. Boyd, and I. I. Beilis, Phys. Plasmas **8**, 5315 (2001).
[9] S. Barral, K. Makowski, Z. Peradzynski, N. Gascon, and M. Dudeck, Phys. Plasmas **10**, 4137 (2003).
[10] E. Ahedo, J. M. Gallardo, and M. Martinez-Sanchez, Phys. Plasmas **10**, 3397 (2003); E. Ahedo, *ibid.* **9**, 4340 (2002).
[11] E. Ahedo and D. Escobar, J. Appl. Phys. **96**, 983 (2004).
[12] A. V. Zharinov and Yu. S. Popov, Sov. Phys. Tech. Phys. **12**, 208 (1967).
[13] A. I. Morozov and V. V. Savel'ev, Plasma Phys. Rep. **27**, 570 (2001); A. I. Morozov, Sov. Phys. Dokl. **10**, 775 (1966).
[14] N. Gascon, M. Dudeck, and S. Barral, Phys. Plasmas **10**, 4123 (2003).
[15] D. Staack, Y. Raitses, and N. J. Fisch, Appl. Phys. Lett. **84**, 3028 (2004).
[16] Y. Raitses, D. Staack, M. Keidar, and N. J. Fisch, Phys. Plasmas **12**, 057104 (2005).
[17] A. Smirnov, Y. Raitses, and N. J. Fisch, Phys. Plasmas **11**, 4922 (2004).
[18] A. Dunaevsky, Y. Raitses, and N. J. Fisch, Phys. Plasmas **10**, 2574 (2003).
[19] N. Meeazan and M. Cappelli, Phys. Rev. E **66**, 036401 (2002).
[20] W. X. Wang, M. Okamoto, N. Nakajima, S. Murakami, and N. Ohybu, Nucl. Fusion **37**, 1445 (1997).
[21] D. Staack, Y. Raitses, and N. J. Fisch, Rev. Sci. Instrum. **75**, 393 (2004).
[22] L. Dorf, Y. Raitses, and N. J. Fisch, Rev. Sci. Instrum. **75**, 1255 (2004).
[23] Y. Raitses, L. Dorf, A. Litvak, and N. J. Fisch, J. Appl. Phys. **88**, 1263 (2000).
[24] A. Smirnov, Y. Raitses, and N. J. Fisch, J. Appl. Phys. **95**, 2283 (2004).
[25] Yu. M. Kagan and V. I. Perel, Sov. Phys. Tech. Phys. **13**, 1348 (1969).
[26] V. Kim, J. Propul. Power **14**, 736 (1998).
[27] I. Kaganovich, M. Misina, S. V. Berzhnoi, and R. Gijbels, Phys. Rev. E **61**, 1875 (2000).
[28] M. J. Kushner, IEEE Trans. Plasma Sci. **PS-13**, 6 (1985).
[29] J. E. Pollard, D. E. Diamant, V. Khaims, L. Wethman, D. Q. King, and K. H. de Grys, *Proceedings of the 37th Joint Propulsion Conference, July, 2001, Salt Lake City, Utah* (American Institute of Aeronautics and Astronautics, Reston, VA, 2001), AIAA paper No. 2001-3351; M. L. Walker, R. Hofer, and A. Gallimore, *Proceedings of the 38th Joint Propulsion Conference, July, 2002, Indianapolis, IN* (American Institute of Aeronautics and Astronautics, Reston, VA, 2002), AIAA paper No. 2002-4109.
[30] L. B. King and A. D. Gallimore, J. Propul. Power **16**, 1086 (2001).
[31] D. Sydorenko and A. Smolyakov (private communications, 2004, 2005).
[32] Ch. Sack and H. Schamel, Phys. Rep. **156**, 311 (1987).
[33] M. Keidar and I. D. Boyd, J. Appl. Phys. **86**, 1 (1999).
[34] A. Cohen-Zur, A. Fruchtman, J. Askenazy, and A. Gany, *Proceedings of the 28th International Electric Propulsion Conference, Toulouse, France* (Electric Rocket Propulsion Society, Cleveland, OH, 2003), IEPC 2003-063.
[35] I. D. Boyd and J. T. Yim, J. Appl. Phys. **95**, 4575 (2004).
[36] E. Trussoni, K. Tsinganos, and C. Sauty, Astron. Astrophys. **325**, 1099 (1997).
[37] V. A. Osherovich, C. J. Farrugia, and L. F. Burlaga, J. Geophys. Res., [Space Phys.] **100**, 12307 (1995).
[38] L. N. Hau, T. D. Phan, B. Sonnerup, and G. Paschmann, Geophys. Res. Lett. **20**, 2255 (1993).
[39] A. Fruchtman (private communications, 2003, 2004).
[40] A. Fruchtman and N. J. Fisch, Phys. Plasmas **8**, 56 (2001).
[41] A. Fruchtman, N. J. Fisch, and Y. Raitses, Phys. Plasmas **8**, 1048 (2001).
[42] Y. Raitses, M. Keidar, D. Staack, and N. J. Fisch, J. Appl. Phys. **92**, 4906 (2002).
[43] J. D. Swift and M. J. R. Schwar, *Electrostatic Probes For Plasma Diagnostics* (Elsevier, New York, 1969).
[44] Schmidt, in *Plasma Diagnostics*, edited by W. Lochte-Holtgreven (Amsterdam, North-Holland, 1968).
[45] D. Bohm, E. H. S. Burhop, and H. S. W. Massey, *The Characteristics of Electrical Discharges in Magnetic Fields*, edited by A. Guthrie and R. K. Wakerling (McGraw-Hill, New York, 1949).
[46] J. E. Allen, R. L. F. Boyd, and P. Reynolds, Proc. Phys. Soc. London, Sect. B **70**, 297 (1957).
[47] S. H. Lamb, Phys. Fluids **8**, 73 (1965).
[48] H. M. Mott-Smith and I. Langmuir, Phys. Rev. **28**, 727 (1926).
[49] I. B. Bernstein and I. N. Rabinowitz, Phys. Fluids **2**, 112 (1959).
[50] J. G. Laframboise, UTIAS Rep. 100 (University of Toronto, Toronto, Canada, 1966).
[51] C. Steinbrüchel, J. Vac. Sci. Technol. A **8**, 1663 (1990).
[52] R. R. Hofer and R. S. Jankovsky, *Proceedings of the 28th International Electric Propulsion Conference, March 2003, Toulouse, France* (Electric Rocket Propulsion Society, Cleveland, OH, 2003), IEPC paper 2003-142.
[53] A. I. Morozov, A. I. Bugrova, A. V. Desyatskov, and V. K. Kharchevnikov, Plasma Phys. Rep. **22**, 302 (1996).

Downloaded 18 Jul 2005 to 198.35.4.202. Redistribution subject to AIP license or copyright, see http://pop.aip.org/pop/copyright.jsp